Available online at www.sciencedirect.com
ScienceDirect
Journal of the European Ceramic Society 27 (2007) 157–163
www.elsevier.com/locate/jeurceramsoc

Microstructures and material properties of fibrous HAp/Al_2O_3–ZrO_2 composites fabricated by multi-pass extrusion process

Byong-Taek Lee [a,*], Chi-Woo Lee [a], Asit Kumar Gain [a], Ho-Yeon Song [b]

[a] *School of Advanced Materials Engineering, Kongju National University, 182, Shinkwan-dong, Kongju City, Chungnam 314-701, South Korea*
[b] *Department of Microbiology, School of Medicine, Soonchunhyang University, 366-1, Ssangyoung-dong, Cheonan-city, Chungnam 330-090, South Korea*

Received 30 November 2005; received in revised form 3 February 2006; accepted 17 February 2006
Available online 9 May 2006

Abstract

Fibrous HAp/Al_2O_3–ZrO_2 composites were fabricated using the multi-pass extrusion process. In the 3rd and 4th passed extrusion bodies, fibrous microstructures were obtained. The 3rd and 4th passed Al_2O_3–ZrO_2 cores used as reinforcement, were about 35 and 4.5 μm in diameter, respectively. In the bodies sintered at over 1400 °C, the HAp decomposed and was transformed to β-TCP and TTCP, in which large numbers of pores were observed. The values of bending strength, Vickers hardness and fracture toughness of the 3rd passed HAp/Al_2O_3–ZrO_2 composites were 178 MPa, 325 Hv, and 3.4 MPa $m^{1/2}$, respectively while the values of the 4th passed bodies were 190 MPa, 405 Hv and 3.8 MPa $m^{1/2}$.

Keyword: Hydroxyapatite composite; Mechanical properties; Extrusion; Al_2O_3; ZrO_2

1. Introduction

Recently, calcium phosphate based bioceramics have become materials of interest for use in hard tissue applications due to their excellent biocompatibility.[1,2] Calcium phosphates exist in various phases depending on the temperature and the presence of water.[3] Among these phases, hydroxyapatite (HAp, $Ca_{10}(PO_4)_6(OH)_2$) has been considered one of the most important bioceramics for medical and dental applications such as dental implants, orthopedics, bone filler and drug delivery systems because of its excellent biocompatibility, similarity in composition to bone mineral and biological affinity with bone tissue as well as its stability in body fluid.[4–7] However, it shows low mechanical strength and fracture toughness.[8–10] Unfortunately, the fracture toughness of the HAp ceramic does not exceed a value of about 1 MPa $m^{1/2}$ as compared to 2–12 MPa $m^{1/2}$ for human bone.[11] The main region showing the low fracture toughness of HAp is basically due to the absence of fracture toughening mechanism. In general, its flexural bending strength is strongly related to the microstructural characteristic, such as the presence of secondary phases, β and α tricalcium phosphate and the percentage of porosity.[12] Therefore, to improve the fracture toughness of HAp, many researchers have been focused on microstructure control having nano-sized structures and fibrous composites, which were dispersed with a secondary phase such as ZrO_2, Al_2O_3. In our previous work on the multi-extrusion process called the fibrous monolithic process, the fracture toughness was remarkably improved due to the multi-toughening mechanism such as the crack bridging using the fibrous microstructure, microcracking due to the mismatch of thermal expansion coefficients between the Al_2O_3 and the *m*-ZrO_2 phase and the phase transformation toughening of *t*-ZrO_2.[13,14]

In this work, fibrous HAp/Al_2O_3–ZrO_2 composites were fabricated using the multi-pass extrusion process. The material properties and microstructure, depending on the sintering temperatures and number of extrusion passes were investigated in detail using X-ray diffraction (XRD) and back-scattered electron scanning electron microscope (BSE-SEM) techniques.

2. Experimental procedure

To fabricate the HAp/Al_2O_3–ZrO_2 composites, HAp (about 45 μm, Strem chemical, USA), Al_2O_3 (about 0.3 μm, AKP-50, Sumitomo, Japan) and *m*-ZrO_2 (about 70 nm, *m*-ZrO_2, Tosho,

* Corresponding author. Tel.: +82 41 850 8677; fax: +82 41 858 2993.
E-mail address: lbt@kongju.ac.kr (B.-T. Lee).

0955-2219/$ – see front matter © 2006 Published by Elsevier Ltd.
doi:10.1016/j.jeurceramsoc.2006.02.038

Japan) powders were used as a starting material. And also, ethylene vinyl acetate (EVA) (ELVAX 210 and 250, Dupont, USA) and stearic acid ($CH_3(CH_2)_{16}COOH$, Daejung Chemicals & Metals Co., Korea) were added as binder and lubricant, respectively. First, the Al_2O_3 and *m*-ZrO_2 powders (volume fraction 75:25) were homogeneously mixed in ethanol by the ball mill process using Al_2O_3 ball as a milling media. After mixing, the milling media Al_2O_3 balls were separated and dried on a hot plate while stirring. The ball milled mixture powders (75 vol.% Al_2O_3/25vol.% *m*-ZrO_2)/EVA/stearic acid (volume fraction 60:30:10) were mixed using a shear mixer (Shina Platec. Co., Korea). The mixture was used to make the rod by the extrusion process. On the other hand, to make the tube, HAp/EVA/stearic acid (volume fraction 50:40:10) were homogeneously mixed using a shear mixer. This rod and tube were assembled to make a feed role and extruded in a heated die to make the 1st passed filaments about 3.5 mm in diameter. The 1st passed filaments were cut and loaded in a steel die and extruded to make the 2nd passed filaments. The 3rd passed and 4th passed filaments were produced in the same way using the 2nd and 3rd passed filaments, respectively. To remove the EVA binder, the burning-out process was carried out at 700 °C for 2 h in a N_2 atmosphere. Finally, the pressureless sintering process was carried out at difference temperatures ranging from 1000 to 1550 °C for 2 h in an air atmosphere.

The relative density was measured by the Archimedes method with an immersion medium of water. To measure the Vickers hardness and fracture toughness, the 3.5 mm diameter cylindrical shape samples were cut about 4 mm in length and polished them using up to 1 μm paste. The average Vickers hardness was measured by indenting with a load of 2.5 kg (10 points/sample). To prepare the bending test samples, 3.4 mm in diameter, the bulk samples were cut 35 mm in length and measured by a 4-point bending method with a span length of 10 mm and crosshead speed of 0.1 mm/min, using a universal testing machine (Unitech^{TM}, R&B, Korea). The fracture toughness was calculated by the indentation method using a load of 10 kg. Microstructures were examined using a back-scattered electron scanning electron microscope (JEOL-JSM 5410, Japan) technique. The crystal phases were analyzed by X-ray diffraction (D/MAX-250).

3. Results and discussion

Fig. 1 shows the cross-sectional BSE-SEM microstructures of HAp/Al_2O_3–ZrO_2 composites depending on the number of the extrusion passes. In Fig. 1(a), the 1st passed extruded bodies consisted of a core shell structure. The core part with bright contrast, 2.4 mm in diameter, was Al_2O_3–ZrO_2, while the dark contrast shell part, with a 0.5 thickness was the HAp phase. However, as

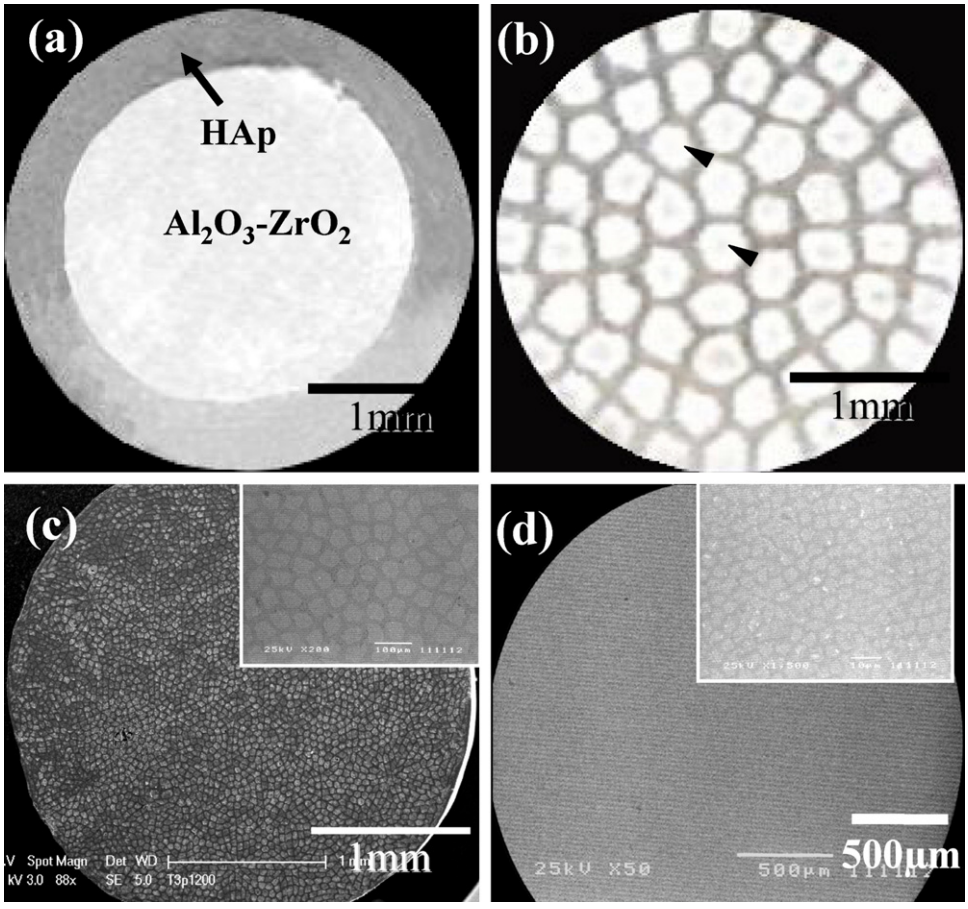

Fig. 1. BSE-SEM micrographs of cross-sectional HAp/Al_2O_3–ZrO_2 filaments: (a) 1st passed; (b) 2nd passed; (c) 3rd passed; (d) 4th passed; and (e and f) enlarged portions of (c) and (d).

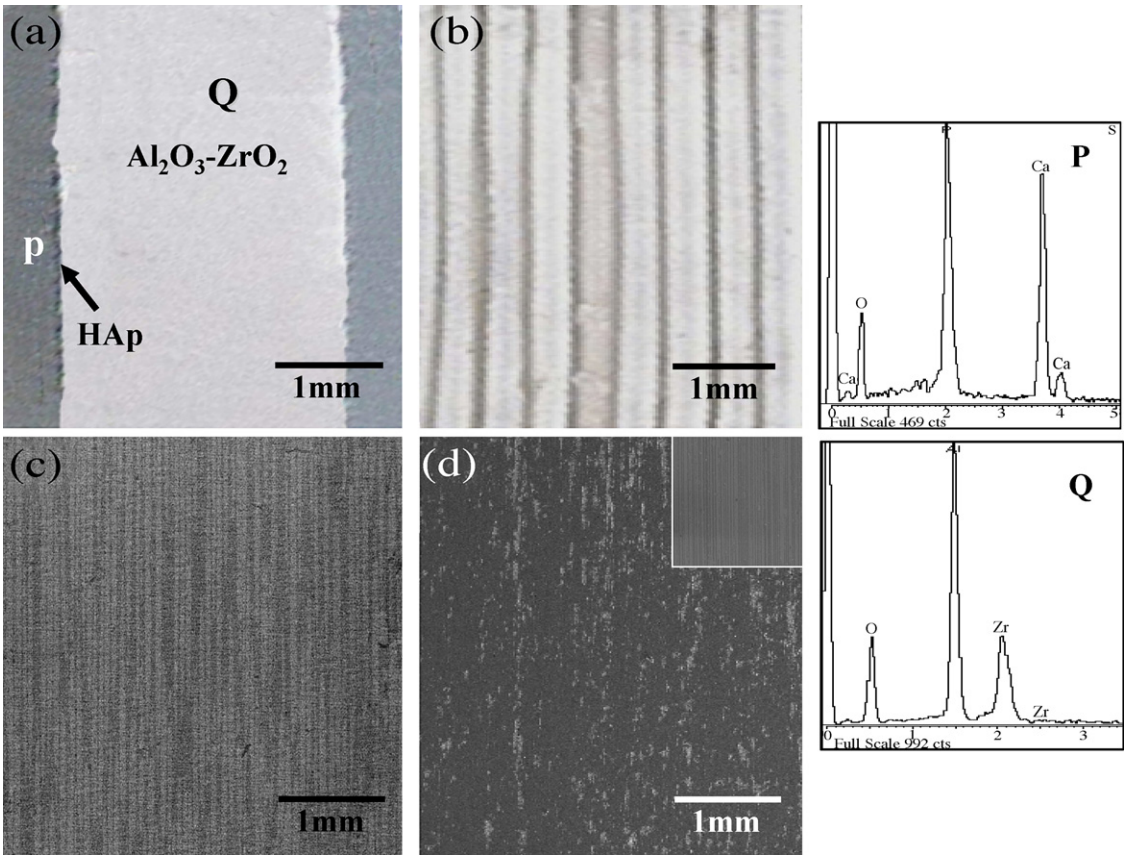

Fig. 2. BSE-SEM micrographs of longitudinal direction of extruded filaments: (a) 1st passed; (b) 2nd passed; (c) 3rd passed; (d) 4th passed and EDS profiles (P and Q).

the number of extrusion passes increased, the core/shell structure formed homogeneously, as indicated by arrowheads shown in Fig. 1(b). The diameter of the reinforced Al_2O_3–ZrO_2 cores in the 2nd passed extruded bodies was 260 μm. Furthermore, in the sample of the 3rd and 4th passed extruded bodies as shown in the inserted enlarged images (c) and (d), the microstructure became a fine network structure as the number of extrusion passes increased. In the 3rd passed sample, the diameter of the reinforced Al_2O_3–ZrO_2 core was about 40 μm in diameter while the diameter of the 4th passed sample was about 4.5 μm.

Fig. 2 shows the BSE-SEM micrographs of longitudinal: (a) 1st passed; (b) 2nd passed; and (c) 3rd passed extruded bodies. In the 1st passed sample as shown in Fig. 2(a), the shell (HAp) and the core Al_2O_3–ZrO_2 were clearly observed with dark contrast and bright contrast, respectively. On the other hand, in the 2nd passed sample, the alternative fibrous microstructure was well controlled. The thickness of the core part was about 260 μm. In the 3rd passed sample, the fibrous microstructure was observed with as a continuous, straight line without any shrinkage cavities and microcracks. However, in 4th passed sample, the fibrous microstructure was too fine as shown in the high-resolution image. From the EDS profiles taken from the P and Q region of SEM image (a), it was confirmed that the shell and core part were HAp and Al_2O_3–ZrO_2 phases, respectively.

Fig. 3 shows the SEM micrographs of: (a) HAp/Al_2O_3–ZrO_2 composite sintered at 1200 °C and (b and c) enlarged image of the Al_2O_3–ZrO_2 and HAp regions. In Fig. 3(a and c), the HAp shell region was about 1 μm in thick and was comprised of fine grains with dense microstructures ranging from 200 to 250 nm in diameter. However, in the Al_2O_3–ZrO_2 core region in Fig. 3(b), many fine pores were clearly observed as indicated with arrowheads due to the low sintering temperature. The large faint, fine white grains were Al_2O_3 and ZrO_2 phase, respectively. The average grains sizes of the Al_2O_3 and ZrO_2 phases were 200 and 90 nm in diameter, respectively. This observation indicated that there was no excessive grain growth due to the low sintering temperature.

Fig. 4 shows the XRD profiles of: (a) raw Al_2O_3–ZrO_2 and (b) HAp powders and HAp/Al_2O_3–ZrO_2 composite sintered at (c) 1000 °C; (d) 1200 °C; and (e) 1400 °C. In XRD profiles, which were sintered at (c) 1000 °C and (d) 1200 °C, only Al_2O_3 and *m*-ZrO_2 phases were detected as well as HAp phase. However, as the sintering temperature increased up to 1400 °C (e), β-TCP peaks were detected with sharp, strong intensity and also a weak TTCP phase was detected due to decomposition of the HAp phase.

Fig. 5 shows the relative density and bending strength of the 3rd and 4th passed HAp/Al_2O_3–ZrO_2 composites depending on the sintering temperature. In both samples, the bending strength and relative density increased as the sintering temperature increased. The bending strength of the bodies sintered at 1000 °C was low due to the low sintering temperature.

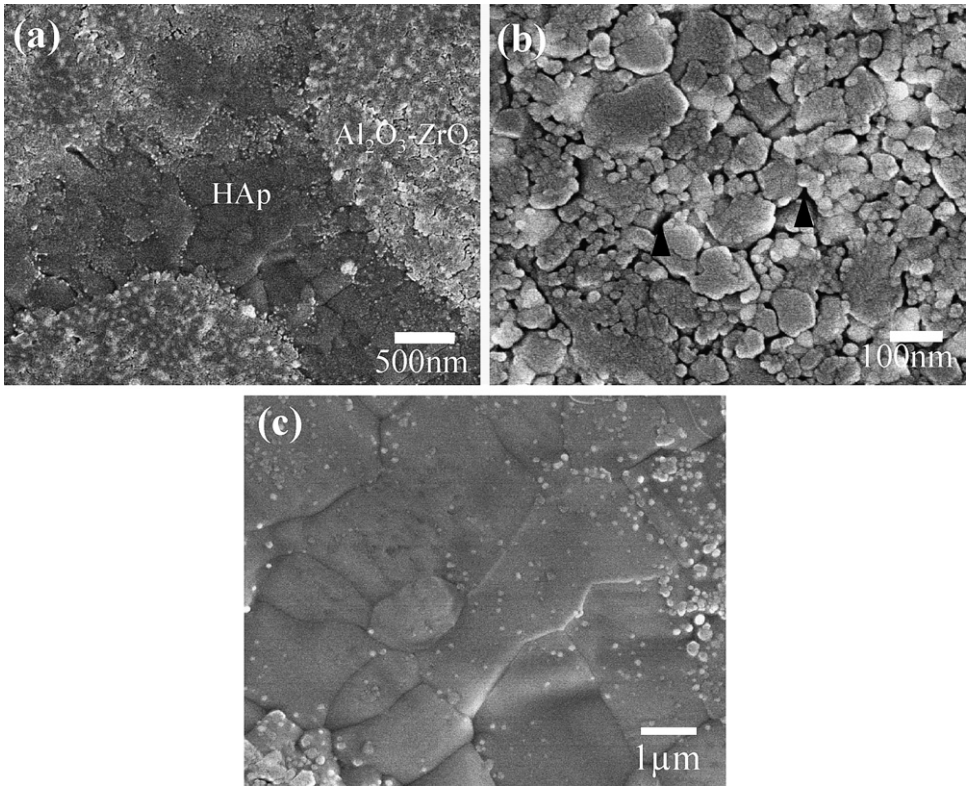

Fig. 3. SEM micrographs of: (a) the 3rd passed HAp/Al_2O_3–ZrO_2 composites; (b and c) enlarged Al_2O_3–ZrO_2 and HAp regions sintered at 1200 °C.

However, as the sintering temperature increased from 1000 to 1200 °C, the bending strength value was increased remarkably in both samples due to the sintered matrix HAp phase. The values of bending strength in the 3rd and 4th passed samples were 158 and 175 MPa respectively, while the relative densities were 97and 95%, respectively. Furthermore, as increasing the sintering temperature up to 1550 °C, the values of bending strength also increased due to densification of the Al_2O_3–ZrO_2 phases. However, the bending strength was comparatively low because the HAp phase decomposed at higher temperature. The values of bending strength in the 3rd and 4th passed bodies sintered at 1550 °C were about 178 and 190 MPa, respectively, but the relative densities were almost the same at about 96%.

Fig. 6 shows the Vickers hardness and fracture toughness of the 3rd and 4th passed HAp/Al_2O_3–ZrO_2 composites depending on the sintering temperature. In both samples, the Vickers hardness and fracture toughness also increased as the sintering temperature increased. The fracture toughness of the 3rd and 4th passed sample sintered at 1200 °C was about 1.7 and 2.5 MPa $m^{1/2}$, respectively. W. Suchanek et al. reported that the fracture toughness of the monolithic HAp did not exceed the value of about 1 MPa $m^{1/2}$. However, the values of frac-

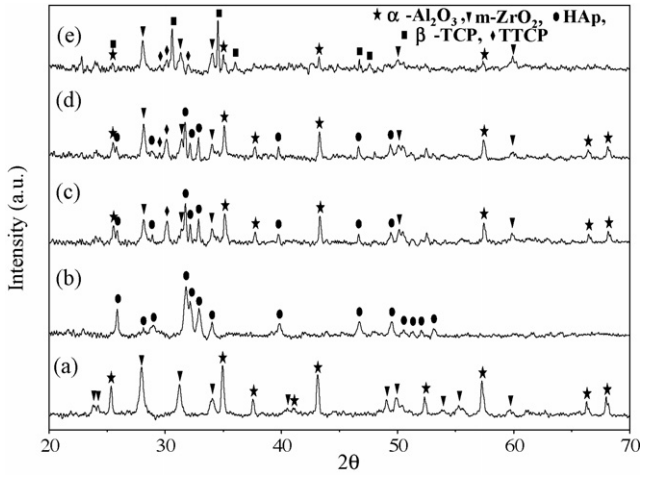

Fig. 4. XRD profiles of: (a) Al_2O_3–ZrO_2; (b) HAp raw powders; (c) 1000 °C; (d) 1200 °C; and (e) 1400 °C sintered HAp/Al_2O_3–ZrO_2 composites.

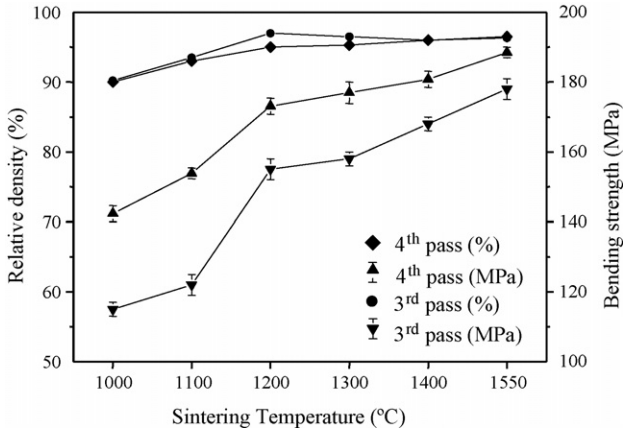

Fig. 5. Relative density and bending strength of 3rd and 4th passed HAp/Al_2O_3–ZrO_2 composites depending on sintering temperature.

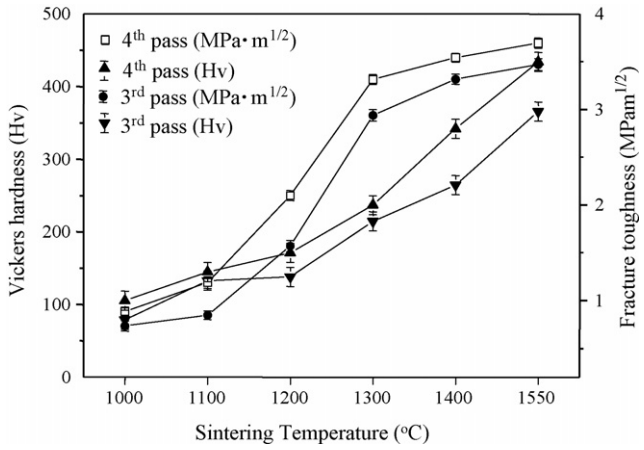

Fig. 6. Vickers hardness and Fracture toughness of 3rd and 4th passed $HAp/Al_2O_3–ZrO_2$ composites depending on sintering temperature.

ture toughness and Vickers hardness in the 3rd and 4th passed $HAp/Al_2O_3–ZrO_2$ composites sintered at 1550 °C were 3.4 and 3.8 MPa $m^{1/2}$ and 325 Hv and 405 Hv, respectively. The values of the fracture toughness, bending strength and Vickers hardness in the 4th passed sample were comparatively higher than those of the 3rd passed sample due to the control of the fine, fibrous microstructure.

Fig. 7 shows the cross sectional SEM fracture surfaces of the 3rd passed $HAp/Al_2O_3–ZrO_2$ composites (a and c) sintered at 1200 °C and 1400 °C and enlarged images (b) and (d) of SEM images (a and c). From the low magnification SEM image Fig. 7(a and c) the fracture surface of $HAp/Al_2O_3–ZrO_2$ composites showed ladle shape and very rough surface. It looks like the fracture morphology of natural wood. However, cross sectional $Al_2O_3–ZrO_2$ continuous fibers, 40 μm in diameter, were observed as shown in Fig. 7(b and d). Between the HAp shell and fibrous $Al_2O_3–ZrO_2$ core, some microcracks were observed as indicated by arrowheads in Fig. 7(b). This formation of microcracks occured during the fracture of bulk body. However, after sintering at 1400 °C, in the HAp matrix, many pores were observed as indicated by arrowheads in Fig. 7(d) due to the formation of β-TCP and TTCP phases.

Fig. 8(a and c) shows the cross sectional SEM fracture surfaces of the 4th passed $HAp/Al_2O_3–ZrO_2$ composites sintered at 1200 and 1400 °C and their enlarged images (b and d), respectively. The fracture surface of the 4th passed $HAp/Al_2O_3–ZrO_2$ composites showed a rough surface, but no the ladle like deep roughness was found as well as microcracks due to the fine fibrous microstructure. However, the fracture surfaces of the 4th passed $HAp/Al_2O_3–ZrO_2$ composites sintered at 1200 °C were comparatively denser than those of samples sintered at 1400 °C. Although a small number of pores about 5 μm were observed as

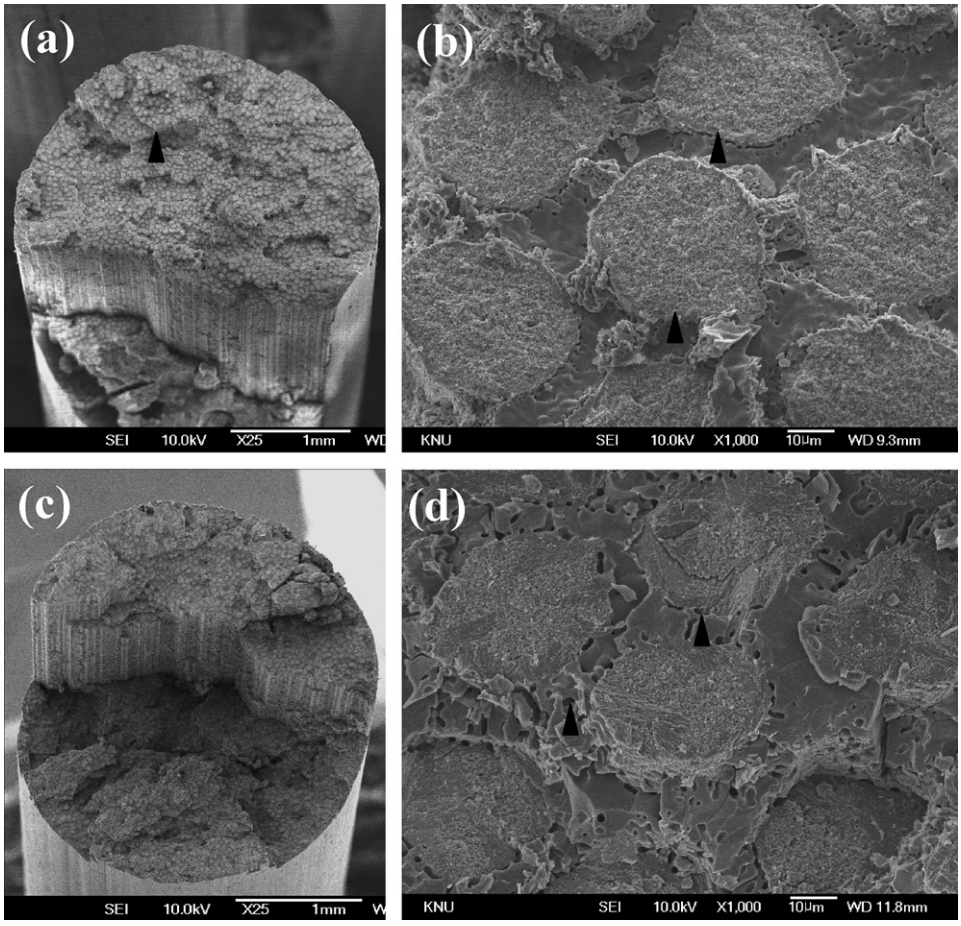

Fig. 7. SEM fracture surfaces of 3rd passed $HAp/Al_2O_3–ZrO_2$ composite depending on sintering temperature: (a and b) 1200 °C and (c and d) 1400 °C.

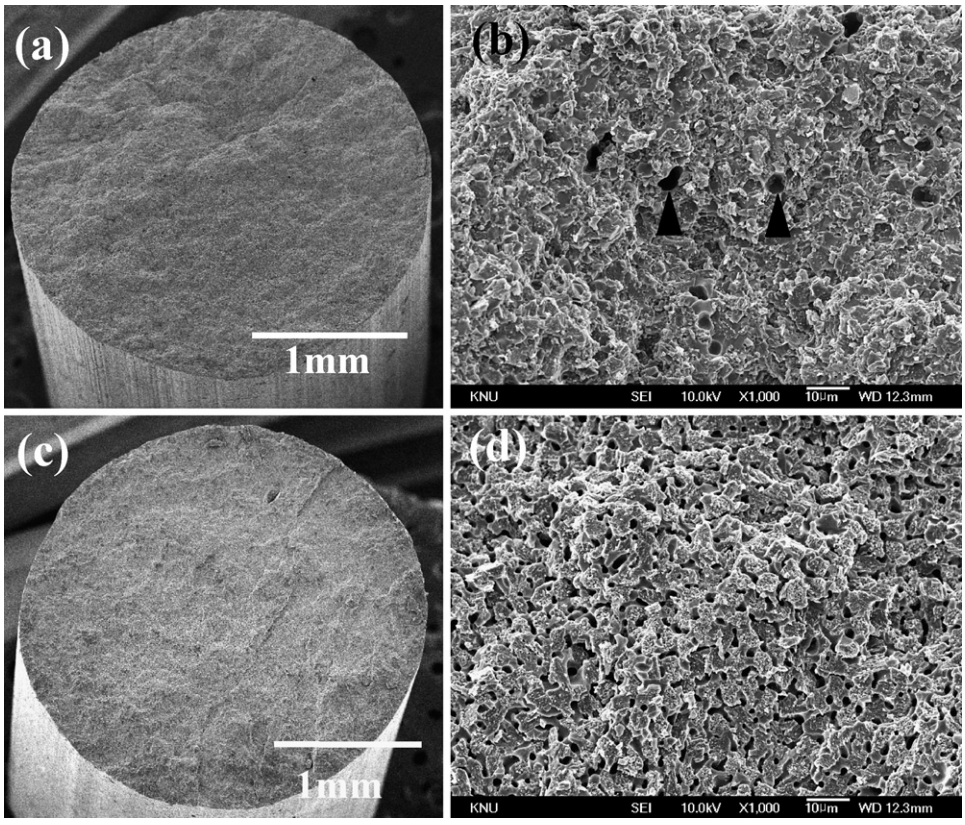

Fig. 8. SEM fracture surfaces of 4th passed HAp/Al_2O_3–ZrO_2 composites depending on sintering temperature: (a and b) 1200 °C and (c and d) 1400 °C.

indicated with an arrowhead as shown in Fig. 8(b), after being sintered at 1400 °C, many pores were clearly observed as shown in Fig. 8(d) due to the decomposition of HAP with β-TCP and TTCP phases. Even though many pores were observed as shown in Fig. 8(d), in the 4th passed sample sintered at 1400 °C, the bending strength increased due to the densification of reinforced Al_2O_3–ZrO_2 core regions.

Fibrous composites having three phases (HAp, Al_2O_3, ZrO_2) were fabricated and their microstructure and material properties were evaluated in this study. As pointed out in Fig. 1, the microstructure of the HAp/Al_2O_3–ZrO_2 composites became fine as the number of extrusion passes increased according to the following equation:

$$r_n = \frac{r_{n-1}}{R^{1/2}}$$

where R is the extrusion ratio and r_n is the resultant radius of the extruded filament after n passes. The 3rd and 4th passed Al_2O_3–ZrO_2 cores as reinforcement were about 35 and 4.5 μm in diameter, respectively. The material properties such as relative density, bending strength and fracture toughness increased as the number of extrusion passes increased. Further, the material properties of fibrous HAp/Al_2O_3–ZrO_2 composites showed higher value than that of monolithic HAp/Al_2O_3–ZrO_2 composite. Rapacz-kmita et al.[15] reported that the fracture toughness of monolithic HAp and HAp-ZrO_2 ceramics were about 0.9–1.1 and 1.1–1.5 MPa $m^{1/2}$, respectively. However, in our present study, the values of the fracture toughness of the 3rd and 4th passed fibrous HAp/Al_2O_3–ZrO_2 composite were about 3.4 and 3.8 MPa $m^{1/2}$, respectively. Those were higher than those of monolithic HAp and HAp-ZrO_2 ceramics due to control of the fibrous microstructure as shown in the fracture surfaces of Fig. 7 as well as in the change in the fracture behavior. From the low magnification SEM image shown in Fig. 7a and c, the fracture surface of the 3rd passed HAp/Al_2O_3–ZrO_2 composites showed ladle shape and very rough surface that looks like the fracture morphology of natural wood were observed due to continuous fiber reinforcement.

4. Conclusion

Fibrous HAp/Al_2O_3–ZrO_2 composites were successfully fabricated using the multi-pass extrusion process. The size and material properties of the reinforced Al_2O_3–ZrO_2 fibers depended strongly on the number of extrusion passes. The size of the Al_2O_3–ZrO_2 fiber dramatically decreased with an increase in the number of extrusion passes. The values of bending strength, Vickers hardness and fracture toughness of the 3rd passed HAp/Al_2O_3–ZrO_2 composites were 178 MPa, 325 Hv, and 3.4 MPa $m^{1/2}$ respectively while the values of the 4th passed bodies were 190 MPa, 405 Hv and 3.8 MPa $m^{1/2}$, respectively. The HAp shell layers showed a fully dense structure without pore after sintering at 1200 °C, while the Al_2O_3–ZrO_2 core had a weak structure due to the low sintering temperature, and some cracks were observed between the HAp matrix and reinforced Al_2O_3–ZrO_2 continuous fibers. On the other hand, in the HAp/Al_2O_3–ZrO_2 composites sintered at 1400 °C, the

densification of Al_2O_3–ZrO_2 cores increased as the sintering temperature increased. However, in the HAp shell, many pores were observed due the thermal decomposition of the HAp phase.

Acknowledgement

This work was supported by NRL research program of the Korean Ministry of Science and Technology.

References

1. Hench, L. L., *Bioceram. J. Am. Ceram. Soc.*, 1998, **81**, 1705–1728.
2. Ryu, H. S., Youn, H. J., Hong, K. S., Chang, B. S., Lee, C. K. and Chung, S. S., An improvement in sintering property of β-tricalcium phosphate by addition of calcium pyrophosphate. *Biomaterials*, 2002, **23**, 909–914.
3. Kalita, S. J., Bose, S., Hosick, H. L. and Bandyopadhhay, A., CaO–P_2O_5–Na_2O-based sintering additives for hydroxyapatite (HAp) ceramics. *Biomaterials*, 2004, **25**, 2331–2339.
4. Brug, K. J. L., Porter, S. and Kellam, J. F., Biomaterial developments for bone tissue engineering. *Biomaterials*, 2000, **21**, 2347–2359.
5. Dash, A. K. and Cudworth, G. C., Therapeutic applications of implantable drug delivery systems. *J. Phamacol. Toxicol. Method*, 1998, **40**, 1–12.
6. Jun, Y. K., Kim, W. H., Kweon, O. K. and Hong, S. H., The fabrication and biochemical evaluation of alumina reinforced calcium phosphate porous implants. *Biomaterials*, 2003, **24**, 3731–3739.
7. Knowles, J. C., Talal, S. and Santos, J. D., Sintering effects in a glass reinforced hydroxyapatite. *Biomaterials*, 1996, **17**, 1437–1442.
8. Chenglim, C., Jingchuan, Z., Zhongda, Y. and Shidong, W., Hydroxyapatite–Ti functionally graded biomaterial fabricated by powder metallurgy. *Mater. Sci. Eng. A*, 1999, **271**, 95–100.
9. Thian, E. S., Huang, J., Best, S. M., Barber, Z. H. and Bonfield, W., Magnetron co-sputtered silicon-containing hydroxyapatite thin films—an in vitro study. *Biomaterials*, 2005, **26**, 2947–2956.
10. Adolfsson, E., Alberiushenning, P. and Hermansson, L., Phase-analysis and thermal-stability of hot isostatically pressed zirconia-hydroxyapatite composites. *J. Am. Ceram. Soc.*, 2000, **83**, 2798–2802.
11. Suchanek, W., Yashima, M., Kakihana, M. and Yashima, M., Hydroxyapatite ceramics with selected sintering additives. *Biomaterials*, 1997, **18**, 923–933.
12. Lopes, M. A., Monterio, F. J. and Santos, J. D., Glass-reinforced hydroxyapatite composites: fracture toughness and hardness dependence on microstructural characteristics. *Biomaterials*, 1999, **20**, 2085–2090.
13. Lee, B. T., Kim, K. H. and Han, J. K., Microstructure and material properties of fibrous Al_2O_3–(m-ZrO_2)/t-ZrO_2 composites fabricated by a fibrous monolithic process. *J. Mater. Res.*, 2004, **19**, 3234–3241.
14. Lee, B. T., Jang, D. H., Kang, I. C. and Lee, C. W., Relationship between microstructures and material properties of novel fibrous Al_2O_3–(m-ZrO_2)/t-ZrO_2 composites. *J. Am. Ceram. Soc.*, 2005, **88**, 2874–2878.
15. Rapacz-Kmita, A., Slosarczyk, A. and Paszkiewicz, Z., Mechanical properties of HAp–ZrO_2 composites. *J. Eur. Ceram. Soc.*, 2006, **26**, 1481–1488.